Experimental and Numerical Results Concerning Ceramic Wicks Applied to LHP Using Water

Paulo Henrique Dias dos Santos, paulosantos@labcet.ufsc.br
Edson Bazzo, ebazzo@emc.ufsc.br
Amir A. M. Oliveira, amir.oliveira@gmail.com
Federal University of Santa Catarina, Department of Mechanical Engineering, LabCET - Laboratory of Combustion and Thermal Systems Engineering - Campus Universitário, 88.040-900, Florianópolis, SC, Brazil

Abstract. *First, the heat and mass transfer in a flat capillary evaporator formed by a single porous wick is analyzed. The wick has a shape of a flat disc and is assembled between the liquid and vapor channels. An external heat input is applied in the upper surface of the wick, where the working fluid evaporates. The mass and heat transfer are modeled using the mass and energy macroscopic conservation equations. The fluid is assumed incompressible, local thermal equilibrium prevails and Darcy's Law is used to model the viscous flow within the porous medium. The model developed allows to verify the effect of the thermal conductivity of the wick in order to calculate the onset of drying of the porous wick. Next, experimental results using ceramic wick (*80% *Mullite and* 20% *Alumina) are reported for a Loop Heat Pipe (LHP) using water as working fluid. The theoretical and experimental results are compared. Besides, further numerical results are also reported for ceramic wick varying its composition: (i)* 50% *Mullite and* 50% *Alumina and (ii)* 20% *Mullite and* 80% *Alumina. Additional experimental works are planned in order to validate the numerical results.*

Keywords: *LHP, Water, Modeling, Thermal Conductivity*

1. Introduction

The electronics industry has grown at a rapid pace seeking the miniaturization and better performance of components. At the scales reached nowadays, the thermal control of electronic equipment has become an important issue. There is a need to develop heat transfer devices that are capable of transferring large amounts of heat with a minimal temperature drop. In this context, Heat Pipes (HP), Loop Heat Pipes (LHP) and Capillary Pumping Loops (CPL) are reliable and feasible alternatives as heat transfer devices. They are passive two-phase devices that utilize the evaporation and condensation of a working fluid to transfer heat. The thermal fluid circulation is accomplished by the capillary forces generated in a porous wick. Therefore, the working fluid pumping does not consume electric power. In this work, only the LHP is studied.

To the authors' knowledge, there are few capillary pumping systems (LHPs and CPLs) using ceramic porous wick as a porous structure of capillary evaporator (Santos *et al.*, 2010; Berti *et al.*, 2010a,b). Most LHP uses polyethylene or metallic porous wicks. It is expected that ceramic wicks become more advantageous, because they are less expensive and easier to machine without damaging the pores in the external surface of the structure. Also the low thermal conductivity can minimize the radial heat leak to the liquid feeding channel, reducing the possibility of boiling in the liquid inlet.

Here in this work, first is developed a mathematical model for the heat and mass transfer problem which occurs within the porous wick of evaporators of capillary pumping systems. This model allows to verify the effect of design variables, such as working fluids, dimensions, permeability, average pore radius and thermal conductivity of the wick, in the performance of the capillary evaporator and it allows for establishing a rigorous criterion for the wick dry-out limit. Next the results obtained with the model are compared with the experimental results obtained with a LHP which uses water as working fluid and a ceramic porous wick as capillary structure.

2. PROBLEM FORMULATION

The geometry of interest here is shown in Fig. 1(a). This figure depicts a capillary evaporator with a bi-layered porous wick (here, both layers are identical and have the same geometrical and thermophysical properties). The operation of the LHP shown in Fig. 1(b) can be described as follows. Heat is supplied to the evaporator so that the liquid saturating the surface pores of the wick evaporates, forming liquid-vapor curved interfaces. The curvature of these interfaces promotes the working fluid circulation by the action of capillary forces. The vapor, which has been generated into the evaporator, flows via the vapor transport line to the condenser, where heat is rejected, causing the condensation of the vapor. Saturated liquid flows back to the evaporator by the capillary-driven flow (essentially Poiseuille flow). Detailed information on the operation, thermodynamic behavior, selection of working fluids and pressure losses of CPLs and LHPs can be found in Maydanik *et al.* (1991); Nikitkin and Cullimore (1998); Maydanik (1999); Ku (1999); Santos and Bazzo (2007).

In this work, the wick is a flat circular disc and is assembled between the liquid feeding channel and the vapor chamber. The upper part of the wick is heated by an external heat flux. After start-up, the evaporation of the working fluid that takes place around the fin occurs in three regimes, depending on the magnitude of the applied heat flux: (1) evaporation in

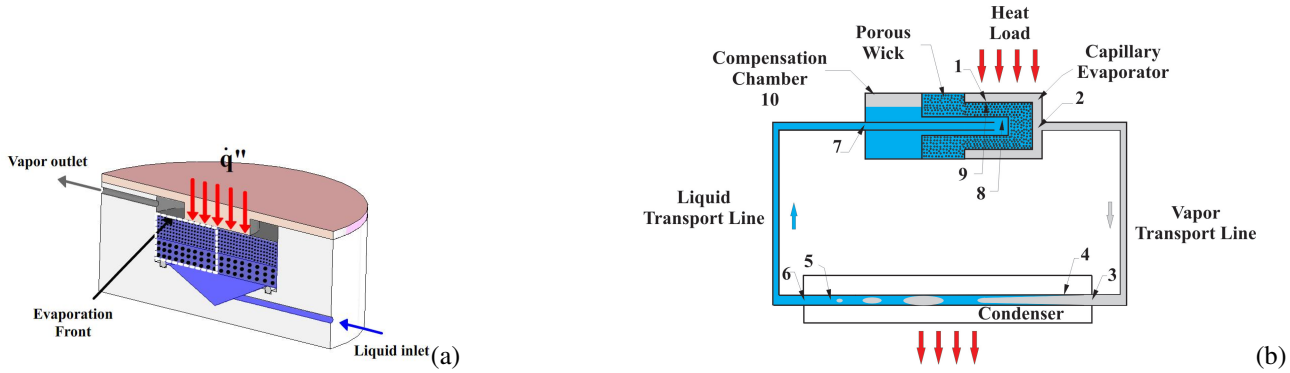

Figure 1. (a) Cut of the flat capillary evaporator with bi-layered wick in the shape of a flat disc (b) Schematic diagram of a typical LHP.

microfilm, (2) evaporation in the external surface of the wick and (3) evaporation within the wick. Here, the evaporation in the external surface of the wick is considered the normal operation mode of a CPL, as verified by Li and Ochterbeck (1999) and assumed also by Cao and Faghri (1994). Also, this evaporation front is assumed sharp. An analysis of the two-phase zone at the dryng front would provide aditional insight into this problem, as shown by Udell (1983) and Hanamura and Kaviany (1995), but this is beyond the scope of the work presented here.

Here, the equations of conservation of energy and mass are cast in cylindrical coordinates with the following assumptions: (1) The process is steady state, (2) The porous layers forming the wick are isotropic and homogeneous, (3) There is a negligible influence of gravity, (4) There are no heat transfer by radiation, (5) The solid phase is inert and stationary, (6) The fluid (liquid and its vapor) is incompressible, (7) The vapor in the vapor chamber is in a saturated state, (8) The thermophysical properties are constant, (9) The solid phase is in local thermal equilibrium with the liquid phase and (10) There are no chemical reactions. The physical domain of interest and the boundary conditions are represented schematically in Fig. 2. Due to the cylindrical symmetry, only the section represented by a dotted line in Fig. 1(a) is modeled.

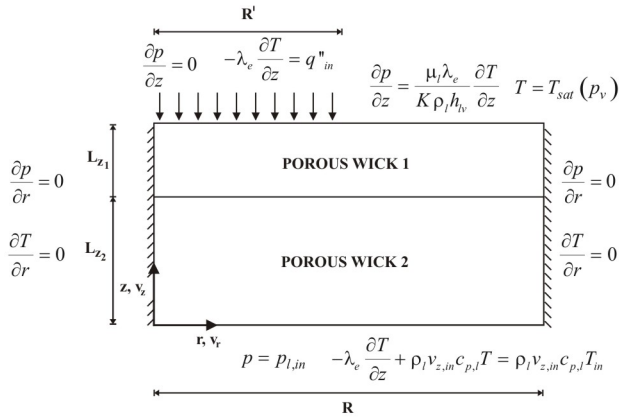

Figure 2. Schematic diagram of the calculation domain and the boundary conditions.

From the hypothesis listed above, the volume-averaged equation for the conservation of mass of liquid in cylindrical coordinates is

$$\frac{1}{r}\frac{\partial}{\partial r}(rv_r)+\frac{\partial v_z}{\partial z}=0. \tag{1}$$

Here, the volume averaged notation is omitted for simplicity. The formulation of the conservation of linear momentum depends on the flow velocity. It has been shown before by Demidov and Yatsenko (1994); Cao and Faghri (1994); Figus *et al.* (1999) that the flow velocity in the application of interest here is small. The pore Reynolds number ($\mathrm{Re}_p = \rho_l v_{z,in} 2r_p/\mu_l$) ranges from 4.0×10^{-5} to 4.0×10^{-4}. Therefore, macroscopic and microscopic (Forscheimer) inertia terms are negligible when compared to the microscopic viscous terms (Kaviany, 1995). Also, since boundary effects penetrate distances that are of the order of a few particle diameters, the macroscopic (Brinkman) viscous term is also neglected. Finally, neglecting the influence of gravity, the r and z components of the equation for the conservation of linear momentum reduce to Darcy's Law, i.e.,

$$v_r=-\frac{K}{\mu}\frac{\partial p}{\partial r},\quad v_z=-\frac{K}{\mu}\frac{\partial p}{\partial z}. \tag{2}$$

Substituting the conservation of momentum in the conservation of mass and assuming constant properties, we obtain a Laplace equation for the pressure, i.e.,

$$\frac{1}{r}\frac{\partial}{\partial r}\left(r\frac{\partial p}{\partial r}\right)+\frac{\partial}{\partial z}\left(\frac{\partial p}{\partial z}\right)=0.$$

The equation for the conservation of the thermal energy is also written neglecting the convective terms. Following Cao and Faghri (1994), the characteristic Peclet number (Pe$=\mathrm{Re}\,\mathrm{Pr}=v_{z,in}R^{'}/\alpha_e$) for the application of interest here is of the order of 10^{-2}. Then, the equation for the conservation of thermal energy, assuming isotropic media and constant properties, is written as

$$\frac{1}{r}\frac{\partial}{\partial r}\left(r\frac{\partial T}{\partial r}\right)+\frac{\partial}{\partial z}\left(\frac{\partial T}{\partial z}\right)=0. \tag{3}$$

For constant properties and isotropic media, the conservation of thermal energy equation reduces to a Laplace equation for the temperature.

Following Fig. 2, the boundary conditions are:

At the surface at $r=0$, cylindrical symmetry requires that

$$\frac{\partial p}{\partial r}=0 \quad \text{and} \quad \frac{\partial T}{\partial r}=0. \tag{4}$$

At the surface at $r=R$, the boundary is assumed impermeable to liquid flow and adiabatic. Then,

$$\frac{\partial p}{\partial r}=0 \quad \text{and} \quad \frac{\partial T}{\partial r}=0. \tag{5}$$

At the inlet surface at $z=0$, the porous wick is fed with a liquid flow with far end temperature $T_{l,in}$, i.e.,

$$p=p_{l,in} \quad \text{and} \quad -\lambda_e\frac{\partial T}{\partial z}+\rho_l v_{z,in}c_pT=\rho_l v_{z,in}c_pT_{l,in} \tag{6}$$

In the volume-averaged sense and assuming local thermal equilibrium between the liquid and solid phases, λ_e is the effective thermal conductivity of the fully liquid saturated porous medium.This temperature boundary condition reflects the continuity of the total normal component of the heat flux vector. Finally, at the outlet surface, two sections are observed. First, underneath the metallic fin ($z=L_z, 0\le r\le R^{'}$)

$$\frac{\partial p}{\partial z}=0 \quad \text{and} \quad -\lambda_e\frac{\partial T}{\partial z}=q_f. \tag{7}$$

Second, assuming that the pore size is not extremely small, i.e., the wick is not a hygroscopic porous medium, from Kelvin's Law, the surface temperature is approximately equal to the vapor saturation temperature in the bulk of the vapor channel. Also, the conduction heat transfer from the fin is responsible for the liquid evaporation. Therefore, the boundary condition at the evaporation surface can be written as,

$$\frac{\partial p}{\partial z}=\frac{\mu\lambda_e}{K\rho_l h_{lv}}\frac{\partial T}{\partial z} \quad \text{and} \quad T=T_{sat}\left(p_v\right). \tag{8}$$

This set of boundary conditions closes the formulation. The total working fluid mass flow rate is given by

$$\dot{m}_{lv}=\left[\int_{R'}^{R}\left(-\frac{K}{\mu}\frac{\partial p}{\partial z}\rho_l\right)rdr\right]_{z=L_z}$$

or

$$\dot{m}_{lv}=\left[\int_{0}^{R}\left(-\frac{K}{\mu}\frac{\partial p}{\partial z}\rho_l\right)rdr\right]_{z=0}. \tag{9}$$

The pressure difference $(p_v-p_{l,in})$ corresponds to the total pressure loss of the LHP components. In all stable operation points, this pressure difference balances exactly the capillary pressure difference across the medium. The total heat transfer rate at the fin is responsible for the liquid evaporation at the outlet surface and part of it flows to the liquid channel. A total energy balance in the wick provides

$$Q_f=q_fA_f=Q_l+Q_{lv}, \tag{10}$$

where Q_f is the applied heat transfer rate at the fin surface.

The heat transfer rate to the liquid channel Q_l, following Eq. 6, is given by,

$$Q_l = \int_0^R \left(-\lambda_e \frac{\partial T}{\partial z} \right) r dr, \;\; at \;\; z = 0. \tag{11}$$

This heat transfer is responsible for raising the incoming flow temperature of the subcooled liquid T_{in} to the inlet porous wick surface value $T(z = 0)$. When Q_l is large, the liquid in the channel can reach the onset of nucleate boiling which is also called a boiling limit for the LHP operation. The boiling limit of interest here is the dryout that occurs underneath the fin, by excess temperature.

In the evaporation front (liquid-vapor interface), located in the external surface of the wick, the pressure difference between the phases is the capillary pressure, which can be expressed by the Young-Laplace's equation. For an averaged pore radius r_p, the capillary pressure becomes maximum when the contact angle between the liquid and the solid approaches zero, i.e., when the wettability of the liquid is maximum. Since the objective here is to explore the maximum pumping capacity, the contact angle is considered equal to zero. At the evaporation interface, the capillary pressure is defined by the liquid and vapor pressures. Then, the average radius of curvature of the liquid-vapor interface adjusts itself in order to balance this capillary pressure, as predicted by Young-Laplace's equation. The minimum possible radius of curvature before drying of the pore is the characteristic radius of the pore. This radius depends on the pore topology and is determined by the choice of material and manufacturing process, i.e., sintering, used to produce the porous wicks. Assuming cylindrical capillaries, the maximum capillary pressure that the wick can withstand is therefore,

$$\Delta p_{cap,max} = p_v - p_{l,\min} = \frac{2\sigma}{r_p} \tag{12}$$

This maximum capillary pressure is related to the threshold for percolation of the non-wetting phase and is commonly identified as the wick bubbling pressure. In the operation of a capillary evaporator, when the pressure losses of the system exceed the maximum capillary pressure, the system fails. Therefore, the capillary limit of a LHP reflects its maximum pumping capacity.

2.1 Nondimensional Equations

Udell (1983) studied the heat and mass transfer in a problem that resembles the operation of a heat pipe. Following Udell (1983), the nondimensional variables are proposed:

$$p_{ref} = \frac{\sigma}{(K/\varepsilon)^{1/2}}, \qquad v_{ref} = \frac{(K\varepsilon)^{1/2}\sigma}{\mu_l L_z}, \qquad q_{ref} = \frac{\lambda_e (T_v - T_l)}{L_z}$$

$$Pe = \frac{\rho_l c_{p,l} (K\varepsilon)^{1/2}\sigma}{\mu_l \lambda_e}, \qquad E_v = \frac{\lambda_e \left(T_v - T_l\right) \mu_l}{\rho_l h_{lv} \left(K\varepsilon\right)^{1/2} \sigma}$$

$$r^* = \frac{r}{R}, \qquad z^* = \frac{z}{L_z}, \qquad T^* = \frac{T - T_l}{T_v - T_l}$$

$$p^* = \frac{p}{p_{ref}}, \qquad v_r^* = \frac{v_r}{v_{ref}}, \qquad v_z^* = \frac{v_z}{v_{ref}}, \qquad q_{in}^* = \frac{q_{in}}{q_{ref}}$$

This nondimensionalization is based on the assumption that $(K/\epsilon)^{1/2}$ provides a suitable order of magnitude for the average pore size. From this estimative, p_{ref} is a reference value for the liquid pressure, v_{ref} is a reference value for the liquid velocity and q_{ref} is a reference value for the heat flux.

The capillary-evaporation number (E_v) is the ratio of conduction heat flux to the energy rate consumed by the evaporation of the capillary-driven liquid flow. This number provides the relation between the nondimensional liquid pressure and temperature gradients at the evaporation surface. Also, the capillary pressure and the pore radius can be cast in nondimensional form as,

$$\Delta p_{cap}^* = \frac{\Delta p_{cap} \left(K/\varepsilon\right)^{1/2}}{\sigma} = \frac{\left(p_v - p_l\right) \left(K/\varepsilon\right)^{1/2}}{\sigma} \tag{13}$$

and

$$r_p^* = \frac{r_p}{\left(K/\varepsilon\right)^{1/2}} \tag{14}$$

2.2 Numerical Results

For the results presented here, water was used as working fluid and a ceramic wick was used as porous wick. The thermodynamic properties of the wick and the working fluid and the main nondimensional parameters are presented in Table 1. In the analysis that follows, the properties were kept constant.

Table 1. Thermophysical properties of the porous wick and working fluid and nondimensional parameters.

	ε (%)	K (m^2)	$\lambda_{e,1}$ (W/m-K)	$\lambda_{e,2}$ (W/m-K)	r_p (μm)
Ceramic	0.5	35×10^{-15}	$4.0 - 8.0$	4.0	$3.0 - 15.0$
	σ (N/m)	$h_l v$ (kJ/kg)	c_p (kJ/kg-K)	ρ ($\mathrm{kg/m^3}$)	μ (kg/m-s)
Water	0.07119	2382	4.18	995.60	0.0007977
	p_{ref} (Pa)	v_{ref} (m/s)	E_v	Pe	L_z/R
	269073	1.181×10^{-3}	0.00143	12.28	0.67

It is expected that an increase in the heat flux at the fin causes an increase in the mass flow rate. Figures 3(a) and (b) present the nondimensional isotherm and heat flux lines for two increasing heat fluxes. Figure 3(a) presents the results for a nondimensional inlet heat flux of 5.0. The fin ends at $r^* = 0.5$. The isotherm with $T^* = 1.0$ ($T = T_v$) is also shown. Note that surface evaporation occurs only in the first few millimeters of the outlet surface, very close to the end of the fin. For the remaining of the fin, the heat flux lines turn around and heat flows right to the liquid channel. As the nondimensional heat flux is increased (Figure 3(b)), an increased amount of heat flows to the outlet surface, causing the liquid evaporation. When the heat flux is increased, the isotherm $T^* = 1.0$ penetrates deeper in the porous wick.

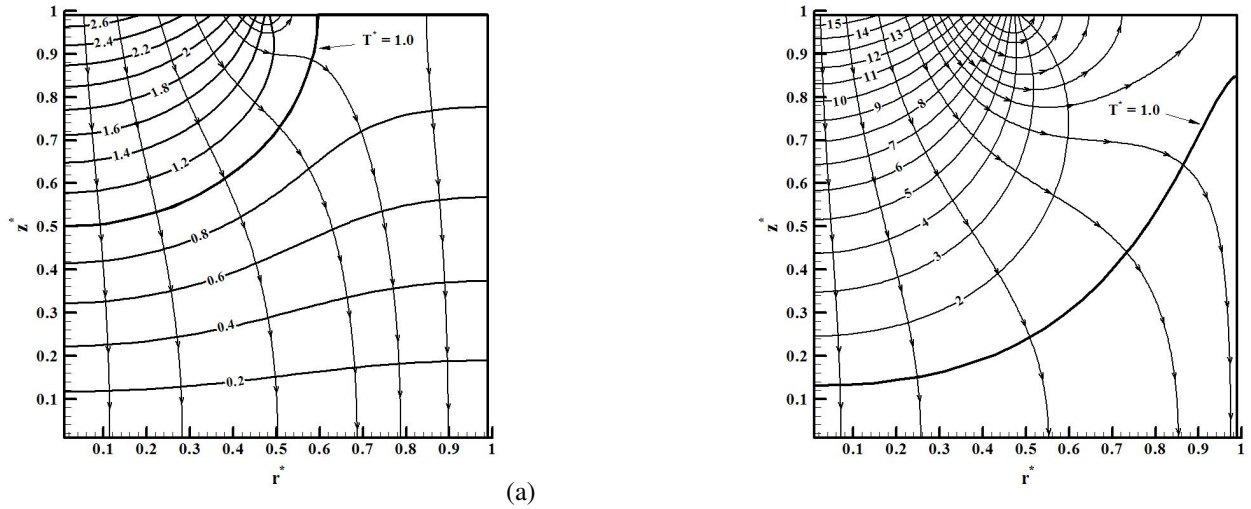

(a) (b)

Figure 3. (a) Nondimensional isotherm and heat flux lines for a nondimensional inlet heat flux of 5.0 ($q_{in} = 2.0 \times 10^4$ $\mathrm{W/m^2}$) and (b) 37.5 ($q_{in} = 1.5 \times 10^5$ $\mathrm{W/m^2}$).

The heat transfer rate imposed in the fin is transferred to the outlet surface, causing evaporation, and also to the inlet surface, resulting in heating of the liquid channel. Both these heat transfer paths have their characteristic thermal resistances. As a result of these thermal resistances, the fin surface reaches a temperature which can be reasonably large in certain conditions. For instance in Fig. 3(b), we observe that for a nondimensional inlet heat flux of 37.5, the fin surface reaches nondimensional temperatures above 15 which are about 14 times above the nondimensional saturation temperature of the fluid (for infinite radius of curvature). Then, a question remains whether the fluid would remain liquid or evaporate under this temperature. This can be tested by observing the capillary pressure at the top surface of the wick and comparing it to the maximum capillary pressure that the wick can sustain.

The maximum capillary pressure that a pore with radius r_p can sustain is,

$$\Delta p_{cap,max} = \frac{2\sigma}{r_p}$$

This can be nondimensionalized using Eq. 13 resulting in,

$$\Delta p^*_{cap,max} = \frac{2\sigma\,(K/\varepsilon)^{1/2}}{\sigma r_p} = \frac{2\,(K/\varepsilon)^{1/2}}{r_p} \tag{15}$$

Note that this maximum nondimensional capillary pressure is a purely geometrical parameter. Therefore, the maximum nondimensional capillary pressure is the one that exists for a pore with radius equal to $2\,(K/\varepsilon)^{1/2}$. When applied to a porous wick, this means that the maximum capillary pressure is the one that occurs when the average radius of the curvature of all menisci exposed to the vapor phase is equal to r_p.

The local nondimensional capillary pressure at the outlet surface is given by equation Eq. 13 (repeated here)

$$\Delta p^*_{cap} = \frac{(p_v - p_l)\,(K/\varepsilon)^{1/2}}{\sigma}$$

where $p_v = p_{sat}(T_v)$ and p_l is the local value of liquid pressure calculated from the improved model, $p_l = p_l(r)$ at $z = L_z$. Here, $\sigma = \sigma(T)$ where T is the porous wick temperature.

Using $p_v = p_{sat}(T_v)$ and p_l obtained from the solution of the model, $p_l = p_l(r)$ at $z = L_z$, Δp^*_{cap} can be calculated and compared to $\Delta p^*_{cap,max}$.

Figure 4(a) presents the nondimensional capillary pressure at the top surface as a function of properties for two heat fluxes, $q^*_{in} = 10.5$ and $q^*_{in} = 5.0$. All properties were kept constant and correspond to the properties of the porous wick with nondimensional average pore radius of 11.34. The horizontal lines represent the maximum nondimensional capillary pressure for each characteristic nondimensional pore size, from 11.34 to 56.69 as shown. We note that for the nondimensional inlet heat flux of 5.0 all media would remain saturated by liquid except those with the larger nondimensional pores of 37.80 and 56.69. For these two sizes, the local capillary pressure exceeds the maximum allowed capillary pressure and, therefore, the region underneath the fin would dry and the evaporation front would seek a new equilibrium position within the wick. This condition in which the front is embedded within the wick has been analyzed by Demidov and Yatsenko (1994); Figus *et al.* (1999); Takahashi (2002); Kaya and Goldak (2006).

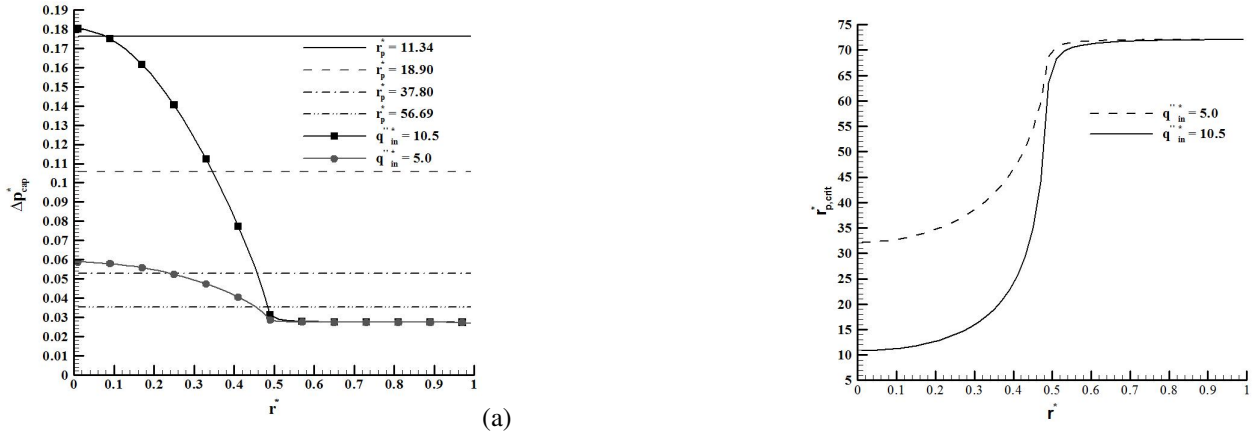

(a) (b)

Figure 4. (a) Nondimensional capillary pressure profiles at $z^* = 1.0$ for different nondimensional averaged radius of curvature and nondimensional inlet heat fluxes and (b) critical nondimensional average radius profiles at $z^* = 1.0$ for two nondimensional inlet heat fluxes.

For a given nondimensional heat flux there will be a local maximum nondimensional average radius needed to avoid the drying of the wick in the region underneath the fin, which will be called critical nondimensional average radius ($r^*_{p,crit}$). From Eq. 13 and 14, this is given by,

$$r^*_{p,crit} = \frac{2\sigma}{(p_v - p_l)\,(K/\varepsilon)^{1/2}} \tag{16}$$

where $p_v = p_{sat}(T_v)$ and p_l is the local value of liquid pressure calculated from the improved model, $p_l = p_l(r)$ at $z = L_z$. Here, $\sigma = \sigma(T)$ where T is the porous wick temperature.

Figures 4(b) depict the curves of critical nondimensional average radius as a function of the nondimensional heat flux in the upper part of the wick ($z^* = 1$). It is noticed in Fig. 4(b) that the minimum critical nondimensional average radius is located in the region underneath the fin at $z^* = 1.0$ and $r^* = 0.0$. Thus, the Fig. 5 presents the critical nondimensional average radius as a function of the nondimensional heat flux at $z^* = 1.0$ and $r^* = 0.0$. The curve shown in this figure represents the capillary limit, *i.e.*, bellow this curve the capillary limit is not reached and there is no vapor breakthrough and above the curve occurs the vapor invasion of the porous wick.

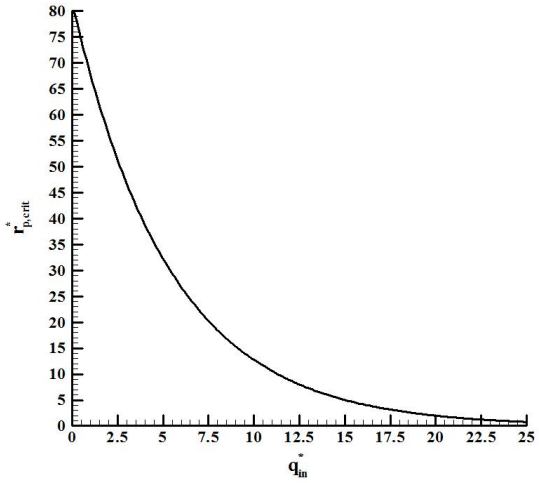

Figure 5. Critical nondimensional average radius at $z^* = 1.0$ and $r^* = 0.0$ as a function of the nondimensional inlet heat flux.

3. EXPERIMENT

In this work one LHP was manufactured and tested in order to evaluate their thermal performance and their applicability in thermal control of microprocessors and electronic components in general. The surface temperatures at the main part of the systems, e.g. evaporator outlet ($T_{Evap,out}$), condenser inlet ($T_{Cond,in}$), condenser outlet ($T_{Cond,out}$), evaporator inlet ($T_{Evap,in}$) and the compensation chamber (T_{CC}) were measured while the thermal load was varied. The LHP used water as working fluid and a ceramic wick in the capillary evaporator. For the heating of the capillary evaporator, electric resistors were used to simulate the heat generation in microprocessors and electronic components. The condenser of the LHP was cooled using water in forced convection.

Figure 6(a) shows the LHP and its capillary evaporator has 10 mm of inner diameter and 25 mm of length, the compensation chamber has the same diameter of the evaporator and length of 50 mm, the transport lines of liquid and vapor have 2.8 mm of inner diameter and the condenser has 120 mm of length. Figure 6(b) shows a view of the evaporator, the compensation chamber and the ceramic wick of the LHP. The ceramic wick applied to LHP has 50% of porosity, 1 to 3 μm pore size distribution and permeability of about 35×10^{-15} m^2. Only the upper side of the wick has four grooves which were machined.

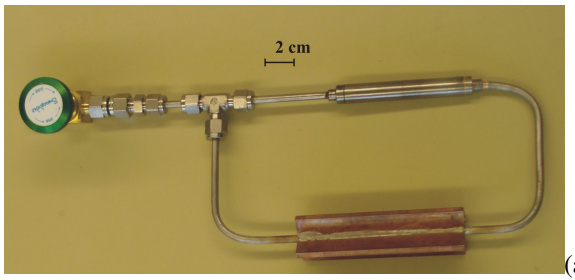

(a)

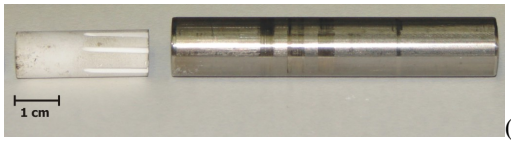

(b)

Figure 6. (a) General view of the LHP and (b) view of the evaporator, the compensation chamber and the ceramic wick of the LHP.

The LHP was first adjusted to the horizontal position and the ambient temperature was set. Once all temperatures of the LHP showed the same value as the ambient temperature ($\Delta T_{max} = 1^o$ C), the first power input step of 5 W was applied to the evaporator. Once all temperatures reached a stationary value (or oscillating stationary value), the power input was increased by steps of 5 W. The electrical power (P_{el}) applied to the cartridge was calculated by measuring the current and the voltage accross it. Assuming no heat losses through the insulation at the heating zone, the applied electrical power is taken as the heat applied to the systems. The performance tests were carried out for power inputs ranging from 5 to 15 W.

Including the accuracy of the temperature sensors and the uncertainties of the data logger, the uncertainty of the temperature is estimated at ± 0.41 ^{o}C. The uncertainty of the electrical power input is estimated at ± 0.12 W including the uncertainty of the power supply unit and the uncertainty of the data logger. Further information concerning the estimative of the experimental uncertainty can be found in Santos (2010).

3.1 Experimental Results

Figure 7 depicts the temperatures of the evaporator outlet ($T_{evap,out}$), condenser inlet ($T_{cond,in}$), condenser outlet ($T_{cond,out}$), evaporator inlet ($T_{evap,in}$) and the compensation chamber (T_{CC}) at horizontal position and heat sink temperature of 20 ^{o}C for stepwise increase in heat transfer rate. The LHP worked satisfactorily in the range from 5 to 15 W, as shown in Fig. 7. The maximum operation temperature was set to 100 ^{o}C for safety reasons. The outlet evaporator temperature reached high temperatures ranging from 60 to 100 ^{o}C, and the temperature difference to the heat sink temperature (20 ^{o}C), varied from 40 to 80 ^{o}C.

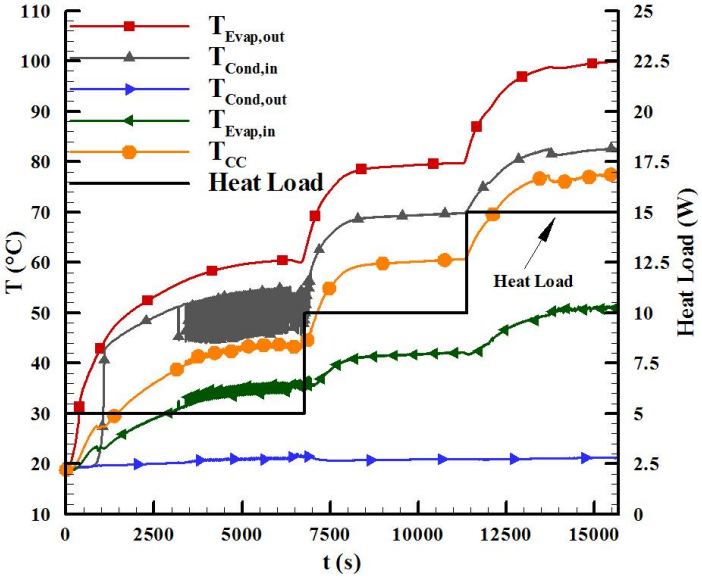

Figure 7. Temperatures of LHP for heat loads increasing at horizontal position and at heat sink temperature of 20 ^{o}C.

4. COMPARISON BETWEEN THE EXPERIMENTAL AND THEORETICAL RESULTS

This section presents a comparison between the experimental and theoretical results obtained with the model. The curves of the critical nondimensional average radius at $z^* = 1.0$ and $r^* = 0.0$ as a function of the nondimensional inlet heat flux are compared to the experimental nondimensional average radius for each heat flux applied to the LHP tested in this work. Figure 8 presents this comparison.

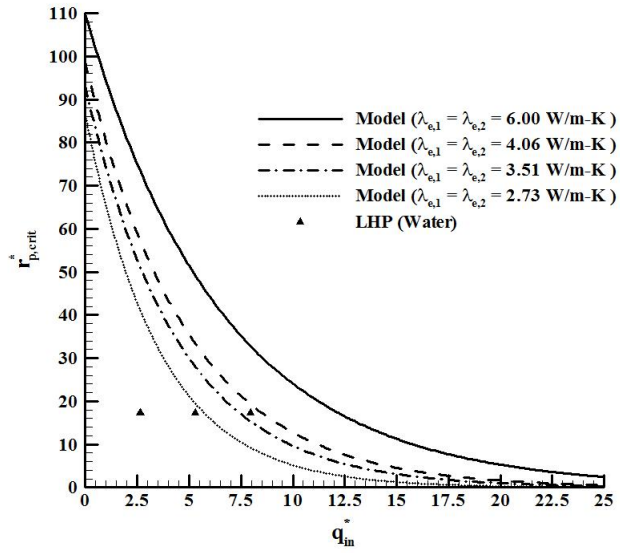

Figure 8. Comparison between the experimental and theoretical results.

The experimental nondimensional average radius was estimated for average pore radius of 3 μm and permeability of

1.5×10^{-14} m^2 (Berti, 2008). The input heat fluxes (q_{in}) for each capillary pumping system tested here were estimated as,

$$q_{in} = \frac{Q_{app}}{N_{fin} A_{fin}},$$

where Q_{app} is the heat transfer rate applied to the capillary evaporator, N_{fin} is the number of fins in the capillary evaporator and A_{fin} is the area of one fin.

The effective thermal conductivity for porous wick saturated with liquid (λ_e) was calculated using the correlation reported by Hadley (1986),

$$\frac{\lambda_e}{\lambda_l} = (1-\alpha_o)\frac{\varepsilon_l\, f_o + \dfrac{\lambda_s}{\lambda_l}\,(1-\varepsilon_l\, f_o)}{1-\varepsilon_l\ (1-f_o) + \dfrac{\lambda_s}{\lambda_l}\varepsilon_l\ (1-f_o)} + \alpha_o \frac{2\left(\dfrac{\lambda_s}{\lambda_l}\right)^2 (1-\varepsilon_l) + (1-2\varepsilon_l)\,\dfrac{\lambda_s}{\lambda_l}}{(2+\varepsilon_l)\,\dfrac{\lambda_s}{\lambda_l} + 1 - \varepsilon_l}$$

where $f_o = 0,8$ and $log\,\alpha_{\,o} = -1,084 - 6,778\,(\varepsilon - 0,298)$. The α_o is valid in the range of $0.298 \leq \varepsilon \ \leq 0.580$.

The input heat fluxes (q_{in}) for the experiments varied from 10.61×10^3 to 31.83×10^3 W/m^2 and they are related to the heat loads from 5 to 15 W for the LHP. The nondimensional input heat fluxes (q^*_{in}) varied from 2.65 to 7.96.

The ceramic wick used in the LHP has 80% of Mullite ($\lambda_{s,Mullite} = 4$ W/m-K) and 20% of Alumina ($\lambda_{s,Alumina} = 40$ W/m-K) and its effective thermal conductivity was estimated as $\lambda_{e,1} = \lambda_{e,2} = 2.73$ W/m-K. Note in Fig. 8 that this ceramic wick presented the lower capillary limit. In this figure, it can be noticed that the LHP has reached the capillary limit, but it continued working for the heat load of 15 W. So, according to the model, the evaporation front invaded the porous wick and stablished a stable position within it.

The ceramic wick composition was varied in order to evaluate the effect of the effective thermal conductivity in the capillary limit. The composition was varied as follow: (i) 50% Mullite and 50% Alumina ($\lambda_{e,1} = \lambda_{e,2} = 3.51$ W/m-K) and (ii) 20% Mullite and 80% Alumina ($\lambda_{e,1} = \lambda_{e,2} = 4.06$ W/m-K). It is also noticed in Fig. 8 that the higher the effective thermal conductivity of the wick the higher the capillary limit. Accordingly, high effective thermal conductivity underneath the fin are desirable for LHPs.

5. CONCLUSIONS

The LHP using water and a ceramic porous wick worked satisfactorily in the range from 5 to 15 W, considering the limit temperature of 100 ^{o}C.

The experimental results were compared with the theoretical results obtained with the model. Despite the LHP has reached the capillary limit, it continued working for the heat load of 15 W. Therefore, according to the model, the evaporation front invaded the porous wick and stablished a stable position within it. However, this comparison should be taken only as a first approximation since the theoretical model does not reproduce completely the geometry of the tested LHP. Nevertheless, the physical trends remain the same. It was also observed that the higher the thermal conductivity underneath the fin the higher the capillary limit.

Finally, further research is still required in order to reduce the operation temperature, evaluating changes related to the properties of the ceramic wick (porosity, pore size and thermal conductivity) and improvements in the whole design of LHP.

6. REFERENCES

Berti, L.F., 2008. *Characterization of Ceramic Wicks for Application in Capillary Pumping Systems (in portuguese)*. Master's thesis, Federal University of Santa Catarina.

Berti, L.F., Santos, P.H.D., Bazzo, E., Hotza, D., Janssen, R. and Rambo, C.R., 2010a. "Porous ceramic structures for capillary pumped loops". *Topics in Chemistry and Material Science*, Vol. 1, pp. 130–137.

Berti, L., Santos, P., Bazzo, E., Janssen, R., Hotza, D. and Rambo, C., 2010b. "Evaluation of permeability of ceramic wick structures for two phase heat transfer devices". *Applied Thermal Engineering*, Vol. 31, pp. 1076–1081.

Cao, Y. and Faghri, A., 1994. "Analytical solution of flow and heat transfer in a porous structure with partial heating and evaporation on the upper surface". *International Journal of Heat and Mass Transfer*, Vol. 37, pp. 1525 – 1533.

Demidov, A.S. and Yatsenko, E.S., 1994. "Investigation of heat and mass transfer in the evaporation zone of a heat pipe operating by the inverted meniscus principle". *International Journal of Heat and Mass Transfer*, Vol. 37, pp. 2155–2163.

Figus, C., Bray, Y.L., Bories, S. and Prat, M., 1999. "Heat and mass transfer with phase change in a porous structure partially heated: continuum model and pore network simulation". *International Journal of Heat and Mass Transfer*, Vol. 42, pp. 2557 –2569.

Hadley, G.R., 1986. "Thermal conductivity of packed metal powders". *International Journal of Heat and Mass Transfer*, Vol. 29, pp. 909–920.

Hanamura, K. and Kaviany, M., 1995. "Propagation of condensation front in steam injection into dry porous media". *International Journal of Heat and Mass Transfer*, Vol. 38, Nř 8, pp. 1377–1386.

Kaviany, M., 1995. *Principles of Heat Transfer in Porous Media*. Springer-Verlag.

Kaya, T. and Goldak, J., 2006. "Numerical analysis of heat and mass transfer in the capillary structure of a loop heat pipe". *International Journal of Heat and Mass Transfer*, Vol. 49, pp. 3211–3220.

Ku, J., 1999. "Operating characteristics of loop heat pipes". In *Proceedings of the 29th International Conference on Enviromental System, 1999-01-2007, Denver, Colorado, USA*.

Li, T. and Ochterbeck, J.M., 1999. "Effect of wick thermal conductivity on startup of a capillary pumped loop evaporator". *AIAA*, Vol. 993446, pp. 10–20.

Maydanik, Y.F., 1999. "State-of-the-art of cpl and lhp technology". In *Proccedings of the 11th International Heat Pipe Conference, Tokyo, Japan*.

Maydanik, Y.F., Fershtater, Y.G. and Goncharov, K.A., 1991. "Capillary-pump loop for the systems of thermal regulation of sapcecraft". In *Proceedings of the 4th European Symposium on Space Environmental and Crontrol Systems, Florance, Italy, pp. 87-92.*

Nikitkin, M. and Cullimore, B., 1998. "Cpl and lhp technologies: What are the differences, what are the similarities?" *SAE Paper*, Vol. No. 981587.

Santos, P.H.D., 2010. *Theoretical and Experimental Study of the Application of a Ceramic Porous Wick in LHP And CPL*. Ph.D. thesis, Federal University of Santa Catarina.

Santos, P.H.D. and Bazzo, E., 2007. "Thermohydraulic analysis of two-phase capillary pumping systems for industrial design and space applications". In *Proccedings of the 19th International Congress of Mechanical Engineering (COBEM), Brasília, Brazil.*

Santos, P.H.D., Bazzo, E., Becker, S., Kulenovic, R. and Mertz, R., 2010. "Development of lhps with ceramic wick". *Applied Thermal Engineering*, Vol. 30, pp. 1784–1789.

Takahashi, A.R., 2002. *Analisys of Heat and Mass Transfer with Phase Change into Porous Wicks Regarding its Optimization for Application in Capillary Pumps (in portuguese)*. Master's thesis, Federal University of Santa Catarina.

Udell, K.S., 1983. "Heat transfer in porous media heated from above with evaporation, condensation and capillary effects". *ASME*, Vol. 105, pp. 485–492.